



Numerical Heat Load Analysis of Hypersonic Missiles for Compressible Fluid Flow

¹Devang Niranjan, ²Dr. Mohammad Zunaid

M. Tech. Scholar, Department of Mechanical Engineering, Delhi Technological University, Delhi, India¹

Professor, Department of Mechanical Engineering, Delhi Technological University, Delhi, India²

Abstract

Hypersonic missiles are a type of missile that is regarded the fastest in the world, and they are currently being researched and developed in various regions of the world. It works with Mach numbers greater than 5. In this study, we examine the behavior of hypersonic missiles operating at a specific height under various flow field conditions at Mach numbers 5, 7, and 10, as well as the behavior of heat transfer loads on the hyperbolic profile structure. The flow architecture and behavior of shock waves are being numerically simulated. This study contributes to an understanding of the design considerations for hypersonic missiles operating at various heights and atmospheric conditions and it will also help in thermal designing of hypersonic vehicles so that proper thermal management can be designed.

Keywords: Heat Load, Fluid Flow, Load Analysis

I. INTRODUCTION

Hypersonic missiles, capable of traveling at speeds exceeding five times the speed of sound, represent a major advancement in modern military technology. However, their incredible velocity presents a significant challenge: excessive heat generation. As the missile travels at such high speeds, the air around it becomes compressed, causing the temperature to rise sharply. These temperatures can reach up to 2,200 degrees Celsius, which poses a risk of damaging or destroying the missile unless properly managed. To tackle this issue, it is essential to understand the mechanisms of heat generation and transfer to the missile [2]. This requires analysing the airflow around the missile and the transition from smooth (laminar) to turbulent flow, which significantly enhances heat transfer. Accurate calculations of the heat load are critical for the design and operation of hypersonic missiles, ensuring they can endure the extreme temperatures and successfully complete their mission. Key studies have made significant contributions to this field. Tauber's 2001 work, "Aerothermodynamic Heating of Hypersonic Vehicles," provides an in-depth analysis of the physical phenomena during hypersonic flight, including shock wave formation and viscous heating, and emphasizes the importance of combining numerical simulations with experimental validation. Another review, "Thermal Protection Systems for Hypersonic Vehicles, examines various TPS materials and technologies, highlighting the need for innovative solutions to balance performance, durability,



maneuverability and reduced interception probability due to their extremely high speed and unpredictable trajectories. Considerable attention was devoted to aerodynamic heating, shock-wave interactions, and propulsion efficiency, all of which significantly influence missile performance during hypersonic flight. Furthermore, the author explored the strategic implications of combining mobility, stealth, and hypersonic speed, which may alter future military doctrines and defense architectures worldwide. Challenges related to thermal protection systems, structural integrity, advanced guidance algorithms, and international security concerns were also analyzed. The study concluded that the convergence of hypersonic and container missile technologies could redefine future combat strategies by enhancing survivability, deployment flexibility, and tactical effectiveness in high-threat environments.

V. T. Le, N. S. Ha, and N. S. Goo in their review paper “*Advanced Sandwich Structures for Thermal Protection Systems in Hypersonic Vehicles*” provided a detailed investigation of lightweight and thermally resistant structural concepts designed for hypersonic aerospace applications. The authors focused on sandwich composite structures that combine low density with high mechanical strength and excellent thermal insulation characteristics, making them suitable for thermal protection systems (TPS) in hypersonic vehicles. The paper reviewed various core materials, including honeycomb, corrugated, lattice, and foam-based structures, along with advanced face-sheet materials such as ceramic matrix composites and carbon-carbon composites. The study emphasized that hypersonic flight generates extremely high aerodynamic heating due to shock-wave compression and viscous dissipation, which necessitates the use of efficient thermal barriers to protect internal systems and structural components. The authors analyzed heat transfer mechanisms, thermo-mechanical behavior, structural stability, and failure modes under severe thermal loading conditions. Additionally, manufacturing methods, material optimization techniques, and multifunctional design approaches were discussed to improve thermal efficiency while minimizing structural weight. The review highlighted that advanced sandwich structures can significantly enhance thermal resistance, mechanical durability, and overall vehicle performance during sustained hypersonic operations. The study concluded that future advancements in material engineering and structural optimization are essential for developing next-generation reusable hypersonic vehicles with improved safety and operational capability.

I. Nompelis, G. V. Candler, M. S. Holden, and T. P. Wadhams in the study “*Real Gas Effects on Hypersonic Shock Wave*” investigated the influence of real gas phenomena on shock-wave behavior in hypersonic flow environments. The paper explained that at extremely high velocities and temperatures encountered during hypersonic flight, air can no longer be treated as a perfect gas because molecular dissociation, ionization, and vibrational excitation become dominant physical processes. The authors analyzed how these thermochemical nonequilibrium effects alter shock-wave structures, pressure distributions, temperature gradients, and aerodynamic heating characteristics around high-speed vehicles. Using computational and



experimental approaches, the study demonstrated that real gas effects significantly influence flow-field properties and heat transfer rates, thereby affecting vehicle performance, stability, and thermal protection requirements. The research highlighted the limitations of conventional perfect-gas assumptions in accurately predicting hypersonic aerodynamics and emphasized the need for advanced numerical models capable of simulating high-temperature gas dynamics. Furthermore, the paper discussed the interaction between shock waves and boundary layers, which can intensify local heating and lead to structural damage if not properly managed. The findings provided valuable insight into the design of hypersonic vehicles, especially in terms of aerodynamic shaping, thermal shielding, and accurate computational fluid dynamics modeling for extreme flight conditions.

S. Kumar and S. P. Mahulikar in the paper “*Aero-Thermal Analysis of Lifting Body Configurations in Hypersonic Flow*” investigated the aerodynamic and thermal behavior of lifting body geometries operating in hypersonic flight regimes. The study focused on the relationship between vehicle configuration and aerothermal performance, emphasizing that the shape of the lifting body significantly affects shock-wave formation, heat transfer distribution, drag characteristics, and overall flight stability. Through computational simulations and analytical evaluations, the authors examined surface temperature variations, stagnation point heating, and pressure distributions under different hypersonic flow conditions. The paper highlighted that lifting body designs can improve aerodynamic efficiency while simultaneously reducing thermal loads compared to conventional blunt-body configurations. However, the study also pointed out that localized heating near leading edges and shock interaction regions remains a major engineering challenge. The researchers analyzed the effects of geometric parameters such as nose radius, body curvature, and angle of attack on aerodynamic heating and lift-to-drag ratio. The work further emphasized the importance of integrating aerodynamic optimization with thermal protection system design to achieve stable and efficient hypersonic flight. The study concluded that properly optimized lifting body configurations can enhance maneuverability, reduce aerodynamic heating intensity, and improve the survivability of future hypersonic aerospace vehicles.

S. P. Mahulikar in the paper “*Theoretical Aerothermal Concepts for Configuration Design of Hypersonic Vehicles*” presented a theoretical framework for designing hypersonic vehicle configurations based on aerothermal principles. The study emphasized that hypersonic vehicle design must simultaneously address aerodynamic performance and thermal management because of the extreme heating generated during high-speed atmospheric flight. The author explained the importance of understanding shock-wave behavior, viscous interactions, boundary-layer effects, and heat-transfer mechanisms in determining optimal vehicle geometry. Various aerodynamic configurations were theoretically analyzed to evaluate their influence on pressure distribution, drag forces, lift generation, and thermal loading. The paper highlighted that blunt-body designs reduce peak thermal loads by creating detached shock

waves, whereas slender-body configurations improve aerodynamic efficiency but experience higher localized heating. The study also discussed entropy generation, energy transfer processes, and thermal equilibrium concepts associated with hypersonic flow fields. Furthermore, the research proposed design methodologies aimed at minimizing aerodynamic heating while maintaining acceptable lift-to-drag characteristics and structural stability. The paper concluded that successful hypersonic vehicle development requires a balanced integration of aerodynamics, thermodynamics, material science, and thermal protection technologies to ensure reliable performance under severe operational conditions.

III. METHODOLOGY

3.1 Geometrical Modelling

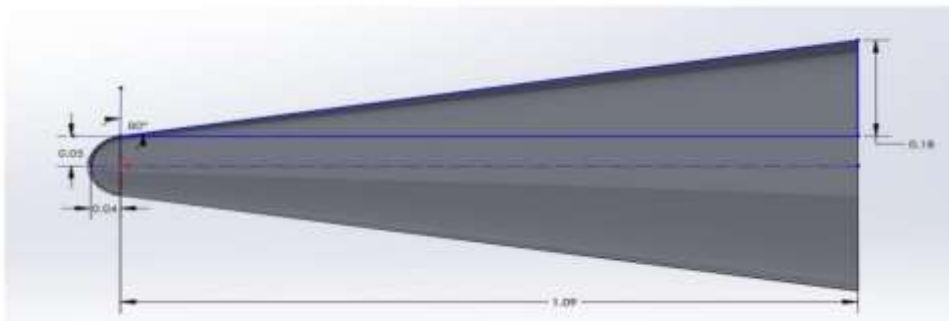


Fig 1: Top View

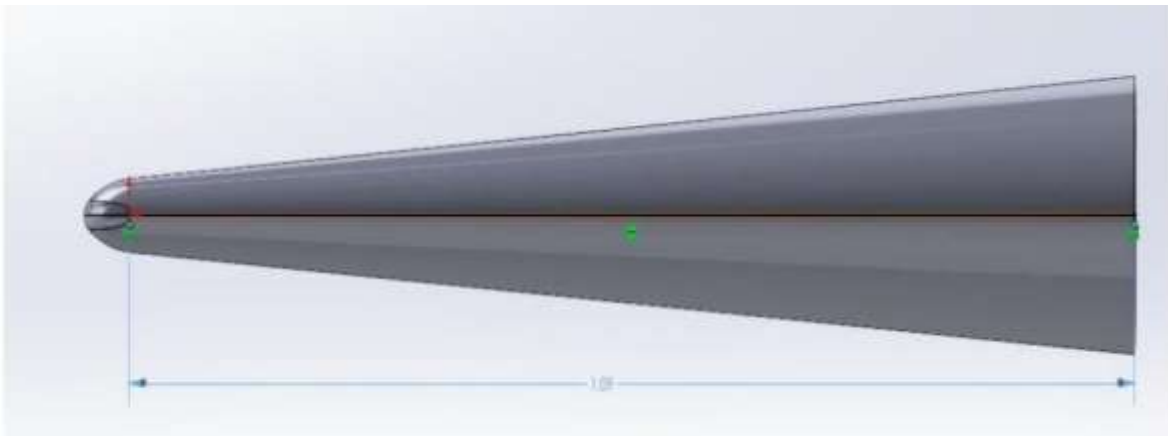


Fig 2: Side View

3.2 Numerical Methodology

Continuity Equation:

$$\frac{\partial \rho}{\partial t} + \frac{\partial(\rho u)}{\partial x} + \frac{\partial(\rho v)}{\partial y} + \frac{\partial(\rho w)}{\partial z} = 0 \tag{1}$$



ρ = the fluid density and u , v and w are the velocity in x , y and z position.

Momentum Equation (Navier-Stokes Equation):

$$\rho \left(\frac{\partial w}{\partial t} + u \frac{\partial w}{\partial x} + v \frac{\partial w}{\partial y} + w \frac{\partial w}{\partial z} \right) = f_x - \frac{\partial P}{\partial z} + \mu \left(\frac{\partial^2 w}{\partial x^2} + \frac{\partial^2 w}{\partial y^2} + \frac{\partial^2 w}{\partial z^2} \right)$$
$$\rho \left(\frac{\partial u}{\partial t} + u \frac{\partial u}{\partial x} + v \frac{\partial u}{\partial y} + w \frac{\partial u}{\partial z} \right) = f_x - \frac{\partial P}{\partial x} + \mu \left(\frac{\partial^2 u}{\partial x^2} + \frac{\partial^2 u}{\partial y^2} + \frac{\partial^2 u}{\partial z^2} \right)$$
$$\rho \left(\frac{\partial v}{\partial t} + u \frac{\partial v}{\partial x} + v \frac{\partial v}{\partial y} + w \frac{\partial v}{\partial z} \right) = f_y - \frac{\partial P}{\partial y} + \mu \left(\frac{\partial^2 v}{\partial x^2} + \frac{\partial^2 v}{\partial y^2} + \frac{\partial^2 v}{\partial z^2} \right)$$

where u , v , and w are the fluid's velocity components at the position (x, y, z) at time t , f is the external force per unit volume of fluid, ρ is the fluid density; P is the pressure, and The constant μ is the kinetic viscosity.

Energy Equation:

$$\rho \left(\frac{\partial w}{\partial t} + u \frac{\partial w}{\partial x} + v \frac{\partial w}{\partial y} + w \frac{\partial w}{\partial z} \right) = f_x - \frac{\partial P}{\partial z} + \mu \left(\frac{\partial^2 w}{\partial x^2} + \frac{\partial^2 w}{\partial y^2} + \frac{\partial^2 w}{\partial z^2} \right)$$
$$\rho \left(\frac{\partial u}{\partial t} + u \frac{\partial u}{\partial x} + v \frac{\partial u}{\partial y} + w \frac{\partial u}{\partial z} \right) = f_x - \frac{\partial P}{\partial x} + \mu \left(\frac{\partial^2 u}{\partial x^2} + \frac{\partial^2 u}{\partial y^2} + \frac{\partial^2 u}{\partial z^2} \right)$$
$$\rho \left(\frac{\partial v}{\partial t} + u \frac{\partial v}{\partial x} + v \frac{\partial v}{\partial y} + w \frac{\partial v}{\partial z} \right) = f_y - \frac{\partial P}{\partial y} + \mu \left(\frac{\partial^2 v}{\partial x^2} + \frac{\partial^2 v}{\partial y^2} + \frac{\partial^2 v}{\partial z^2} \right)$$

where u , v , and w are the fluid's velocity components at the position (x, y, z) at time t , f is the external force per unit volume of fluid, ρ is the fluid density; P is the pressure, and The constant μ is the kinetic viscosity.

3.3 Material Properties

For the analysis we are considering Sic (Silicon Carbide material) for our case because it is having thermal properties that can withstand high temperatures and have additional properties include extreme hardness, good fatigue resistance, high thermal conductivity, low coefficient of thermal expansion. Other materials that can be used are Alumino- Silicate/Nextel 720, Titanium beta alloy etc as per required for different applications and conditions.

Table 1: Thermal properties

Thermal Properties parameters	Values
Density	3100 (kg/m ³)
Thermal Conductivity	120 (W/m-K)
Coefficient of Thermal Expansion	4x10 ⁻⁶ (1/C ^o)
Specific Heat	750 (J/kg-K)
Melting Point	3003 K

3.4 Boundary Conditions

The computation domain considered here for the analysis is considered large enough to ensure that at the boundary we will get free stream effects and for that here we considered Pressure far-field boundary condition at all external boundaries which has a significant role in external compressible flow. The simulation is being performed at steady state condition and considered radiative boundary condition for the internal emissivity of the material to be 0.84. In order to reduce the numerical error due to low pressure, the operating pressure is considered to be zero and ideal gas law has been applied to calculate the air density. Here the analysis is being carried out at the height of 35 km where the pressure is considered to be 768 Pa and the Temperature is kept at 228 K. The specific heat of the air varies with the temperature for different range of temperature, for temperature ranging from (273-550 K) $C_p = 1018.2 \text{ J / k * g - K}$ and for the temperature ranging from (550-2200 K) $[C_p] = a_0 + a_1 \cdot T + a_2 \cdot T^2 + a_3 \cdot T^3 + a_4 \cdot T^4 \text{ J / k * g - K}$ The coefficient values here considered are $a_0 = 874.687$ $a_1 = 0.325431$ $a_2 = - 2.07132 \cdot 10^{-5}$ $a_3 = - 6.63386 \cdot 10^{-8}$ and $a_4 = 2.66 \cdot 10^{-11}$ For thermal conductivity who depends on temperature having the variation as, $k(T) = (1.9942 \cdot 10^{-3} T^{1.5}) / (T + 112)$. The μ (viscosity) variation considered as Sutherland's Law. For the Hypersonic flow simulation, 3-D steady density based, Double precision solver is selected. The results are obtained by solving steady state, compressible RANS equation. Transition-SST turbulence model, using implicit numerical solution scheme. [5]

IV. RESULT AND DISCUSSION

Here the main results are being reported and discussed in terms of Temperature distribution, pressure distribution and Mach number variation across the shock waves and on the wall boundary. The present analysis and effects have been carried out by computational fluid dynamics ANSYS FLUENT 2024 R1. The special attention is paid to nose tip, boundary surface wall and properties across shock waves for different Mach number at height of 35 km.

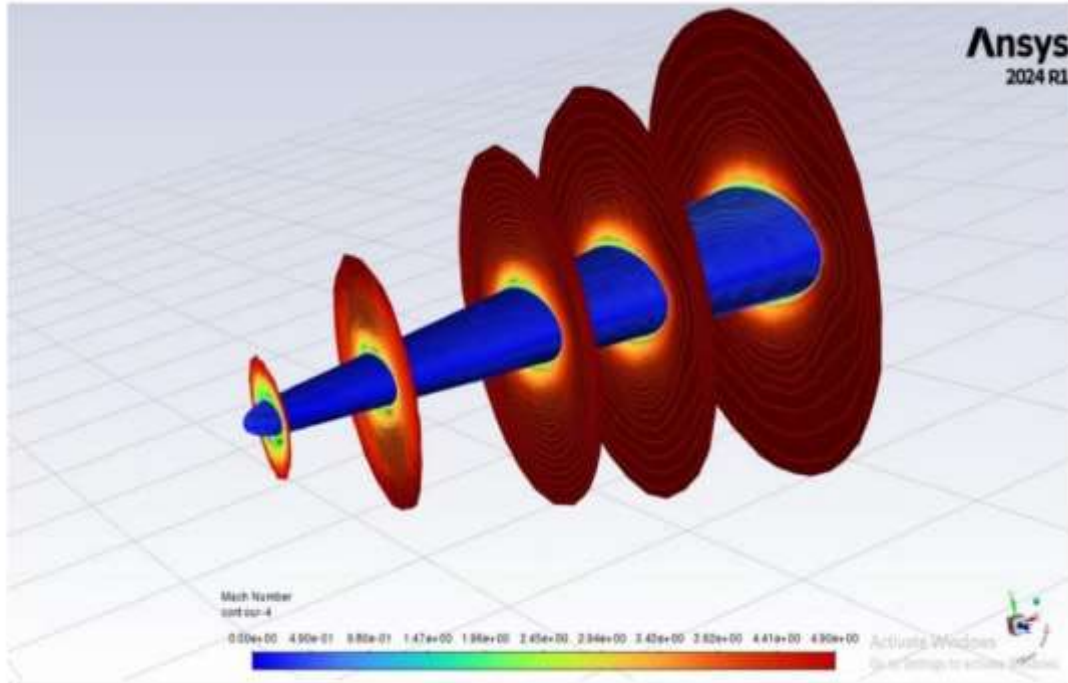


Fig 3: Variation of Mach number around shock wave (M=5)

As can be seen from fig.3, the variation of Mach number around a body of the missile which it experiences as it passes through the shock wave, the enclosure as represented in red colour is moving at a Mach number 5, and the body which is stationary passes through shock wave the Mach number decreases closer to body and that decrease can be seen in the figure. Also, as can be seen the intensity of decrease is more at the tip then at back.

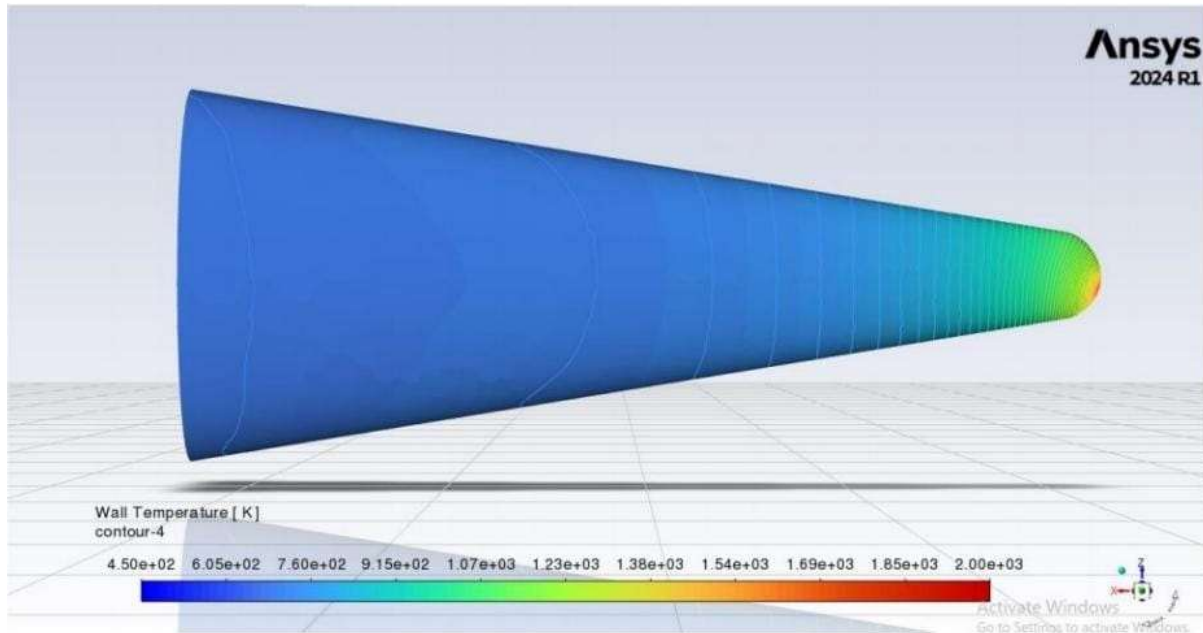


Fig 4: Variation of wall temperature across body (M=5)

Fig 4, shows the variation of wall temperature with respect to length for Mach number 5, the nose tip temperature of the hyperbolic 3D solid body went up to 2,000 K and decreases along the length around the body.

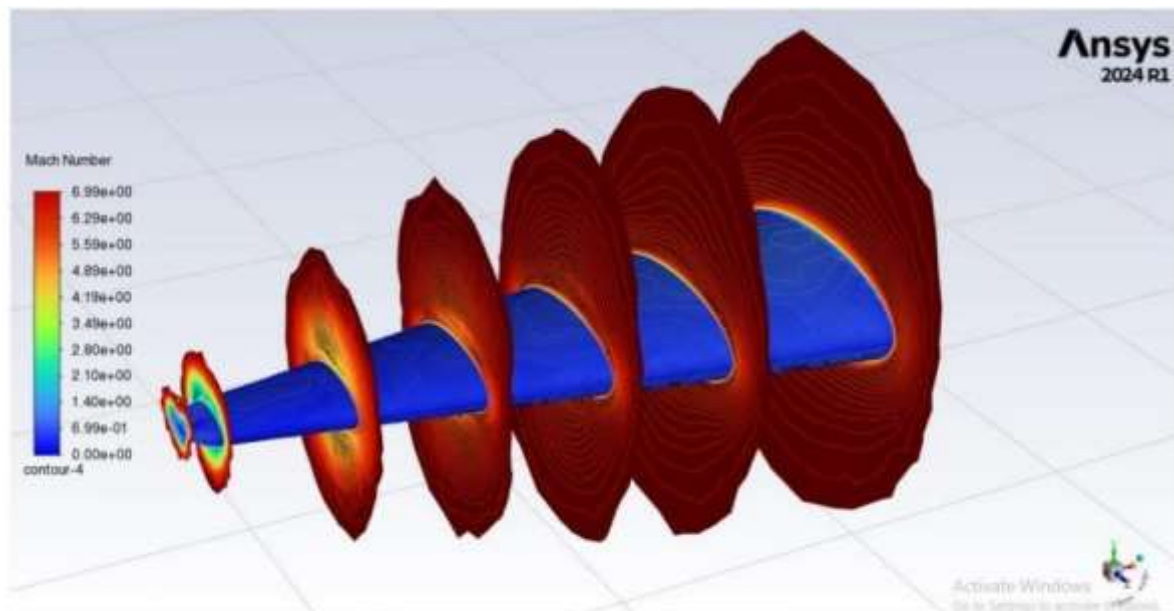


Fig 5: Variation of Mach number around shock wave (M=7)

It can be seen from the fig 5, the variation of Mach number as it passes through the shock wave. The enclosure is at Mach number 7, as compared to Mach number 5 the intensity of decrease of Mach number around the body when the body passes through the shock wave, is more.

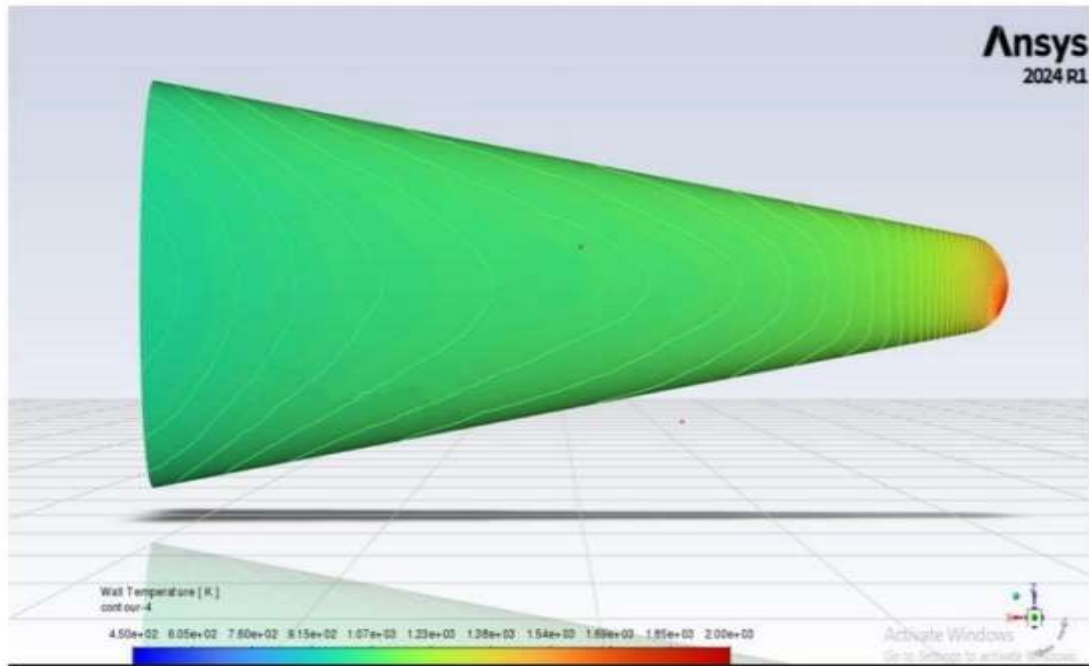


Fig 6: Variation of wall temperature across body (M=7)

Fig 6, shows the variation of wall temperature with respect to length for Mach number 7, the nose tip temperature of the hyperbolic 3D solid body went up to 2,000 K and decreases along the length around the body. But the decrease was lesser as compared to Mach number 5. So the body temperature went up as the Mach number is increased.

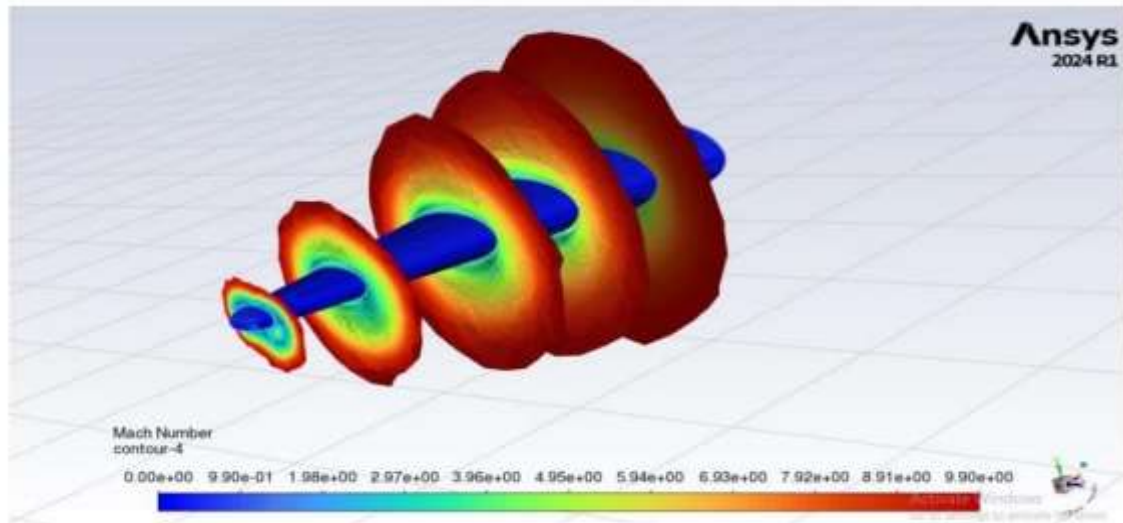


Fig 7: Variation of Mach number around shock wave (M=10)

It can be seen from the fig 7, the variation of Mach number as it passes through the shock wave. The enclosure is at Mach number 10, as compared to Mach number 5 and 7 the intensity of decrease of Mach number around the body when the body passes through the shock wave, is way more, around the nose tip the Mach number decrease is highest as because of formation of normal shock around nose tip.

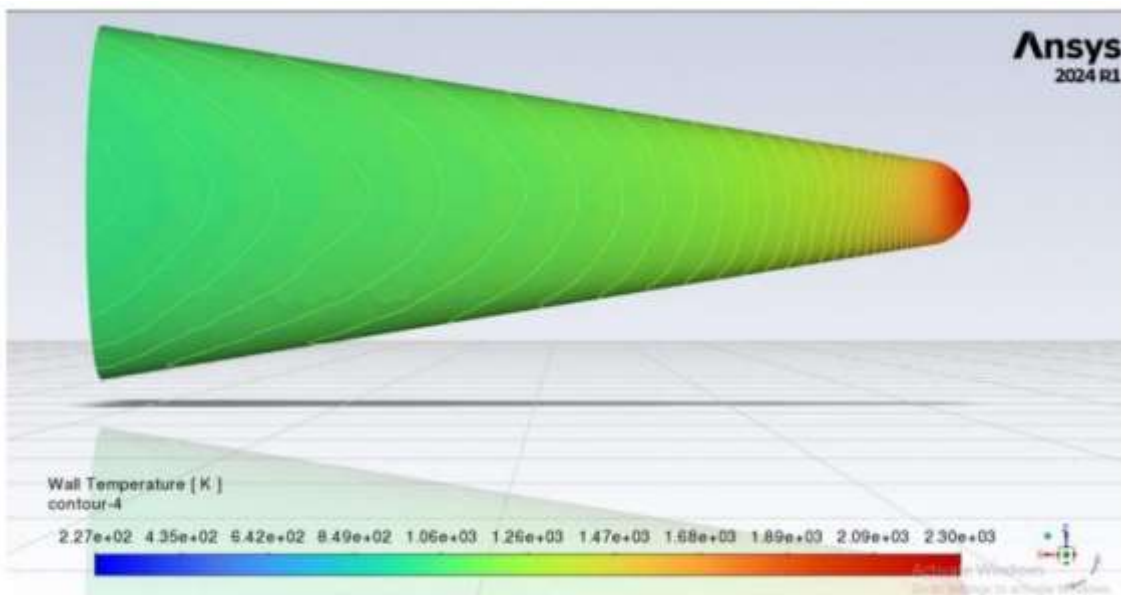


Fig 8: Variation of wall temperature across body (M=10)

Fig 8 , shows the variation of wall temperature with respect to length for Mach number 10, the nose tip temperature of the hyperbolic 3D solid body went up to 2,300 K and decreases along the length around the body. But the decrease was lesser as compared to Mach number 5 or 7. So it can be observed the body temperature went up as the Mach number is increased.

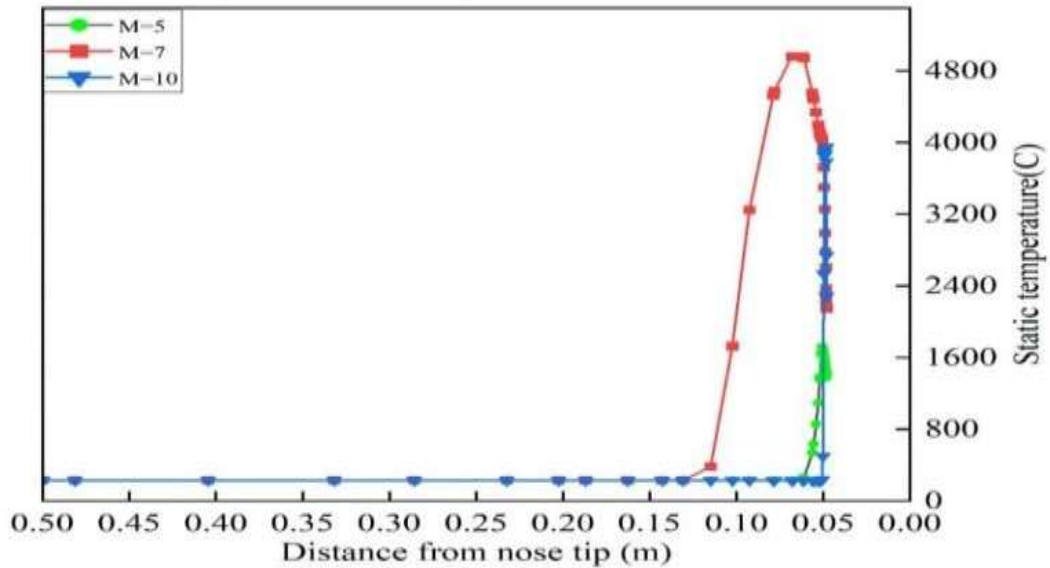


Fig 9: Variation of static temperature along the distance from

For various Mach numbers ($M = 5, 7,$ and 10), the fig 9 shows how the static temperature changes with distance from the nose tip. Near the nose tip, where aerodynamic heating is most severe, it shows a noticeable increase in temperature. The severe impact of shock heating at hypersonic speeds is demonstrated by the fact that this temperature increase becomes more noticeable for higher Mach values. The temperature stabilizes after a given distance from the nose tip, suggesting a zone where the stagnation temperature's effects lessen.

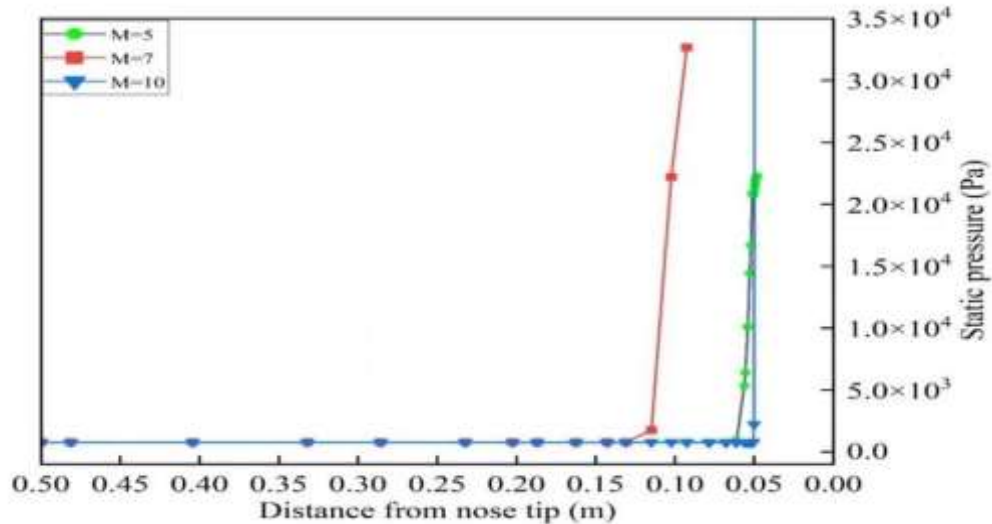


Fig 10: Variation of static pressure along the distance from nose tip

The static pressure distribution for hypersonic flows at Mach numbers 5, 7, and 10 is shown on the fig 10 along the distance from the nose tip. Strong bow shocks form around the nose tip, causing a noticeable pressure increase; higher Mach numbers translate into higher peak pressures. The pressure stabilizes beyond a certain distance from the nose tip, indicating that shock interactions have less of an impact downstream. In hypersonic flow, where shock-induced effects predominate close to stagnation areas, this behavior is typical.

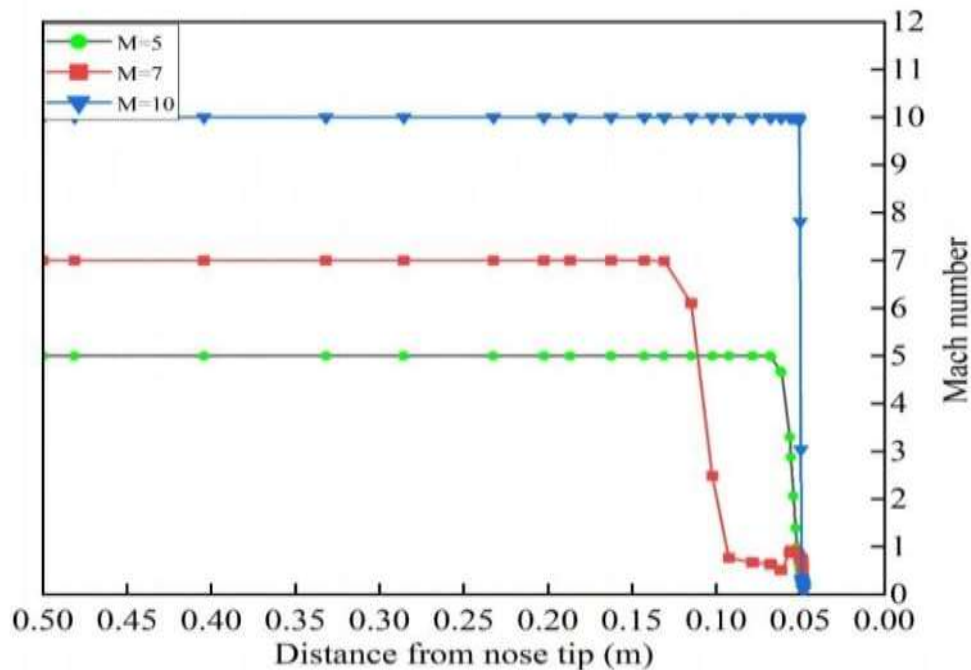


Fig.11: Variation of Mach number along the distance from nose tip



For hypersonic flows at Mach numbers 5, 7, and 10, the fig 11 shows the distribution of Mach numbers along the distance from the nose tip. Near the nose tip, the Mach number decreases sharply due to the deceleration caused by strong shock waves, with the reduction being more pronounced for higher initial Mach numbers. Farther from the nose tip, the flow stabilizes at the respective freestream Mach number, highlighting the dominant role of shock structures in hypersonic regimes near blunt bodies.

V. CONCLUSION

The analysis of temperature distribution, pressure distribution, and Mach number variation across shock waves using ANSYS FLUENT 2024 R1 has provided significant insights into the behaviour of hyperbolic 3D solid bodies at various Mach numbers during flight at an altitude of 35 km. The results indicate distinct relationship between the Mach number and the thermal and aerodynamic characteristics at the nose tip and along the body. It is evident that as the Mach number increases from 5 to 10, the intensity of the Mach number decrease near the nose tip becomes more pronounced, leading to increased thermal loads on the missile.

The data presented highlights that at Mach 5, the nose tip temperature reaches approximately 2,000 K, while increasing the Mach number to 10 raises the peak temperature to around 2,300 K. However, the temperature decreases more gradually with length at Mach 10 compared to Mach 5 and 7. This suggests that although higher Mach numbers result in more nose tip temperatures, the rate of temperature decrease along the body is not proportional to the Mach number increase, warranting further investigation into the thermal protection requirements for missiles operating at these speeds.

Overall, the results underline the importance of understanding shock wave interactions and the corresponding thermal dynamics as these factors significantly impact missile design and operational safety at hypersonic speeds. Future studies should focus on refining computational methods and validating results with experimental data to ensure accurate predictions and effective design strategies.

REFERENCES

- [1] C. L. Herath, "Hypersonic Missile Technology: A Comprehensive Analysis Hypersonic Missile Technology: A Comprehensive Analysis," no. October, pp. 0-23, 2024.
- [2] D. C. Youvan, "Advancements in Hypersonic and Container Missile Technologies: A Vision for Future Warfare," no. March, 2024, doi: 10.13140/RG.2.2.30817.52325.
- [3] V. T. Le, N. S. Ha, and N. S. Goo, "Advanced sandwich structures for thermal protection systems in hypersonic vehicles: A review," *Compos. Part B Eng.*, vol. 226, no. June, p. 109301, 2021, doi: 10.1016/j.compositesb.2021.109301.



International Journal of Research and Technology (IJRT)

International Open-Access, Peer-Reviewed, Refereed, Online Journal

ISSN (Print): 2321-7510 | ISSN (Online): 2321-7529

| An ISO 9001:2015 Certified Journal |

- [4] I. Nompelis, G. V Candler, M. S. Holden, and T. P. Wadhams, "REAL GAS EFFECTS ON HYPERSONIC SHOCK WAVE," no. m, 2003.
- [5] S. Kumar and S. P. Mahulikar, "Aero-thermal analysis of lifting body configurations in hypersonic flow," *Acta Astronaut.*, vol. 126, pp. 382-394, 2016, doi: 10.1016/j.actaastro.2016.05.011.
- [6] S. P. Mahulikar, "Theoretical aerothermal concepts for configuration design of hypersonic vehicles, vol. 9, pp. 681-685, 2005, doi: 10.1016/j.ast.2005.08.006.